Original Article

MOLECULAR METABOLISM

Nuclear Receptor CoRepressors, NCOR1 and SMRT, are required for maintaining systemic metabolic homeostasis

Megan J. Ritter [1,4], Izuki Amano [1,2,4], Norihiro Imai [3], Lorraine Soares De Oliveira [1], Kristen R. Vella [1], Anthony N. Hollenberg [1,*]

ABSTRACT

Objective: The nuclear receptor corepressor 1 (NCOR1) and the silencing mediator of retinoic acid and thyroid hormone (SMRT, also known as NCOR2) play critical and specific roles in nuclear receptor action. NCOR1, both *in vitro* and *in vivo* specifically regulates thyroid hormone (TH) action in the context of individual organs such as the liver, and systemically in the context of the hypothalamic-pituitary-thyroid (HPT) axis. In contrast, selective deletion of SMRT in the liver or globally has shown that it plays very little role in TH signaling. However, both NCOR1 and SMRT have some overlapping roles in hepatic metabolism and lipogenesis. Here, we determine the roles of NCOR1 and SMRT in global physiologic function and find if SMRT could play a compensatory role in the regulation of TH action, globally.

Methods: We used a postnatal deletion strategy to disrupt both NCOR1 and SMRT together in all tissues at 8–9 weeks of age in male and female mice. This was performed using a tamoxifen-inducible Cre recombinase (UBC-Cre-ERT2) to KO (knockout) NCOR1, SMRT, or NCOR1 and SMRT together. We used the same strategy to KO HDAC3 in male and female mice of the same age. Metabolic parameters, gene expression, and thyroid function tests were analyzed.

Results: Surprisingly, adult mice that acquired NCOR1 and SMRT deletion rapidly became hypoglycemic and hypothermic and perished within ten days of deletion of both corepressors. Postnatal deletion of either NCOR1 or SMRT had no impact on mortality. NCOR1/SMRT KO mice rapidly developed hepatosteatosis and mild elevations in liver function tests. Additionally, alterations in lipogenesis, beta oxidation, along with hepatic triglyceride and glycogen levels suggested defects in hepatic metabolism. The intestinal function was intact in the NCOR1/SMRT knockout (KO) mice. The KO of HDAC3 resulted in a distinct phenotype from the NCOR1/SMRT KO mice, whereas none of the HDAC3 KO mice succumbed after tamoxifen injection.

Conclusions: The KO of NCOR1 and SMRT rapidly leads to significant metabolic abnormalities that do not survive — including hypoglycemia, hypothermia, and weight loss. Hepatosteatosis rapidly developed along with alterations in hepatic metabolism suggesting a contribution to the dramatic phenotype from liver injury. Glucose production and absorption were intact in NCOR1/SMRT KO mice, demonstrating a multifactorial process leading to their demise. HDAC3 KO mice have a distinct phenotype from the NCOR1/SMRT KO mice—which implies that NCOR1/SMRT together regulate a critical pathway that is required for survival in adulthood and is separate from HDAC3.

Keywords Gene repression; Thyroid hormone; Nuclear corepressors

1. INTRODUCTION

The nuclear receptor corepressors, NCOR1 and SMRT, are paralog proteins that play critical roles in the regulation of the dynamic signaling properties of nuclear receptors [1–3]. In most cases, NCOR1 and SMRT function to inhibit action by target nuclear receptors in the presence of limited amounts of ligand [4]. They accomplish this primarily by recruiting a multiprotein complex that mediates histone deacetylation [5]. The nuclear receptor interacting domains present in their C-terminus allow for specificity such that NCOR1 is preferentially recruited to the thyroid hormone receptor (TR) isoforms, while the nuclear receptor interacting domains of SMRT have a preference for RAR isoforms [6]. This preference was confirmed *in vivo* with the introduction of a mutation into the NCOR1 allele, which prevents its

[1]Joan and Sanford I. Weill Department of Medicine, Division of Endocrinology, Diabetes and Metabolism, Weill Cornell Medicine, 1300 York Avenue, New York, 10065, USA [2]Department of Integrative Physiology, Gunma University Graduate School of Medicine, Maebashi, 371-8511, Japan [3]Joan and Sanford I. Weill Department of Medicine, Division of Gastroenterology and Hepatology, Weill Cornell Medicine, 1300 York Avenue, New York, 10065, USA

[4] Megan J. Ritter and Izuki Amano contributed equally to the work.

*Corresponding author. E-mail: thollenb@med.cornell.edu (A.N. Hollenberg).

Abbreviations: EF, ejection fraction; HPT, hypothalamic pituitary thyroid axis; IPGTT, intraperitoneal glucose tolerance test; OGTT, oral glucose tolerance test; PTT, pyruvate tolerance test; TG, triglycerides; TH, thyroid hormone; TR, thyroid hormone receptor; TSH, thyroid stimulation hormone

Received April 27, 2021 • Revision received July 20, 2021 • Accepted August 9, 2021 • Available online 12 August 2021

https://doi.org/10.1016/j.molmet.2021.101315

interaction with the TR (NCoRΔID) and leads to a syndrome of increased sensitivity to thyroid hormone globally, as the TR-coactivator interaction is much more strongly favored [7–9]. Furthermore, the introduction of the NCoRΔID allele alleviates the phenotype observed in mice that are designed to express mutant receptors that cause the syndromes of resistance to thyroid hormone [4,10]. Consistent with this, systemic deletion of SMRT from the liver during development or postnatally does not affect thyroid hormone signaling [6,11]. While this previous study strongly supports NCOR1's paramount role in TR action, it is unclear whether further potential redundancy between NCOR1 and SMRT exists in the context of thyroid hormone signaling across a variety of target tissues.

Discerning the systemic actions of NCOR1 and SMRT has been complicated by their requirement for normal embryonic development [12,13]. Complete deletion of NCOR1 during development leads to embryonic lethality from hematologic and neurologic deficits, while deletion of SMRT leads to embryonic lethality because of impaired cardiac ventricular development [12,13]. While these embryonic deletion experiments suggest nonredundant roles for NCOR1 and SMRT, tissue-specific roles suggest otherwise. Importantly, NCOR1 and SMRT mediate at least a portion of their biologic effects through the recruitment and activation of HDAC3, which is also lethal during development, if deleted [14,15]. Interestingly, when NCOR1 and SMRT are deleted together during embryogenesis in the epidermis, lethality occurs because of the lack of an intact external defense barrier, and this phenotype is also observed in epidermal-specific HDAC3 knockout mice [16]. Similarly, NCOR1 and SMRT have overlapping functions to control lipid synthesis which is shared in liver-specific HDAC3 knockout mice [17,18]. Taken together, these studies suggest that NCOR1 and SMRT may have unique roles separate from their ability to recruit HDAC3 and then overlap in function to recruit HDAC3 and maintain its stability as a protein.

To address this fully in the context of the abilities of NCOR1 and SMRT to share redundancy in the regulation of thyroid hormone action, we deleted them from all mouse tissues at 8–9 weeks of age. We used a similar approach to what we have previously used to disrupt SMRT and introduced an inducible NCOR1 allele in all cell types in adulthood where a ubiquitously expressed Cre-driver can be activated by tamoxifen in the presence of conditional NCOR1 and SMRT alleles [6,9]. Thus, we could circumvent the essential developmental functions of NCOR1 and SMRT. Strikingly, beginning immediately after NCOR1/SMRT co-deletion in both male and female 9-week-old mice, hypoglycemia, hypothermia, and a rapidly lethal phenotype developed within ten days. This phenotype was not observed in mice that lacked either NCOR1 or SMRT, individually. Furthermore, when HDAC3 was deleted similarly, all mice survived; though mild weight loss and hypoglycemia developed. Thus, NCOR1 and SMRT appear to have distinct overlapping roles in the regulation of energy metabolism in adults and their co-deletion is not compatible with survival.

2. MATERIALS AND METHODS

2.1. Animal experiments

All experiments were approved by the Beth Israel Deaconess Medical Center and the Weill Cornell Medicine Institutional Animal Care and Use Committee. Mice were housed in a 12-hr light/dark cycle and supplied with food ad libitum. Mice were treated with a previously employed strategy of tamoxifen as described in Figure 1 [3,6] and were euthanized by CO2 asphyxiation followed by cardiac puncture in accordance with the designated timeline. Tissues were rapidly collected and frozen in liquid nitrogen before storage at −80 °C, unless collected for H and E staining.

2.2. Animal generation

Initial breeding of NCOR1$^{loxP/+}$ mice or SMRT$^{loxP/+}$ mice with NCOR1$^{loxP/+}$ mice or SMRT$^{loxP/+}$ mice expressing a tamoxifen-inducible Cre under control of the UBC promoter ((Tg (UBC-Cre/ERT2)1Ejb/J; Jackson Lab) generated the genotypes in Figure 1. Subsequent breeding to generate only NCOR1/SMRT KO and control mice was performed using NCOR1$^{loxP/loxP}$ mice and SMRT$^{loxP/loxP}$ mice. HDAC3$^{loxP/loxP}$ mice were bred to mice that expressed the same UBC-Cre-ERT2. All mice were on a C57/bl6 background.

2.3. Blood chemistry

Hemoglobin, hematocrit, platelet, and white blood cell counts were performed at the Longwood Small Animal Imaging Facility at Beth Israel Deaconess Medical Center in Boston, MA. Samples were processed on the HEMAVET 950FS© (Drew Scientific, UK). Enzymatic assay kits were used to measure plasma insulin levels (89-101-133; Abonva), beta-hydroxybutyrate levels (SBHR100; Stanbio™), aspartate aminotransferase (AST), alanine aminotransferase (ALT) (AST/ALT TR70121/TR71121, Thermo Scientific™), and creatine kinase (CK) (22-022-630; Stanbio™).

2.4. Thyroid function tests

Total plasma T4 levels were measured using AccuDiag™ ELISA Kit (3149–18; Cortez Diagnostics, Inc.). Thyroid-stimulating hormone was measured in plasma using Milliplex MAP Mouse Pituitary Magnetic Bead Panel Mouse (MPTMAG-49K; MilliporeSigma).

2.5. Lipids

Lipids were extracted from frozen specimens with a mixture of chloroform/methanol (2:1) using Folch's method as previously described [19]. Enzymatic assay kits were used to measure plasma and liver concentrations of triglycerides (TG), free fatty acids (FFA), total cholesterol (TC), free cholesterol (FC), and phospholipid (PL) (TG: 994–002891 and 990–02991, TC 999–02601, FC 993–02501, PL 997–01801; FUJIFILM Wako Diagnostics).

2.6. Real-time qPCR

RNA was extracted from the liver using RNA STAT-60 (Fischer Scientific) and 500 ng of RNA was reverse transcribed into cDNA using a kit (SuperScript VILO; Invitrogen). qPCR was performed in duplicate using QuantStudio 6 Flex system. Power SYBR Green Master Mix, Taqman Universal PCR Master Mix, and Taqman gene expression assays were purchased from Thermo Fischer. Relative mRNA levels were calculated using standard-curve methods and were normalized to the level of cyclophilin and 18S to show consistency. Data shown in the figures are all normalized to cyclophilin.

2.7. Western blots

Protein lysates were prepared as previously described [11]. Briefly, 50 mg of the liver was homogenized in 1 mL of cell lysis buffer, 1X proteinase inhibitor, and 1X PMSF. Samples were sonicated on power 4, thrice for 5 s each, and then, spun at 13,200 RPMs for 15 min at 4 °C. Protein concentrations were determined using a BCA reagent (23,227; Pierce™). Protein lysates were resolved in 3–8% Tris-Acetate Novex gel (Invitrogen) for NCOR1, SMRT/NCOR2, and beta-actin or 10% Bis-Tris gel (Invitrogen) for hdac3 and hsp90, and then, transferred to a nitrocellulose membrane. Blots were probed for

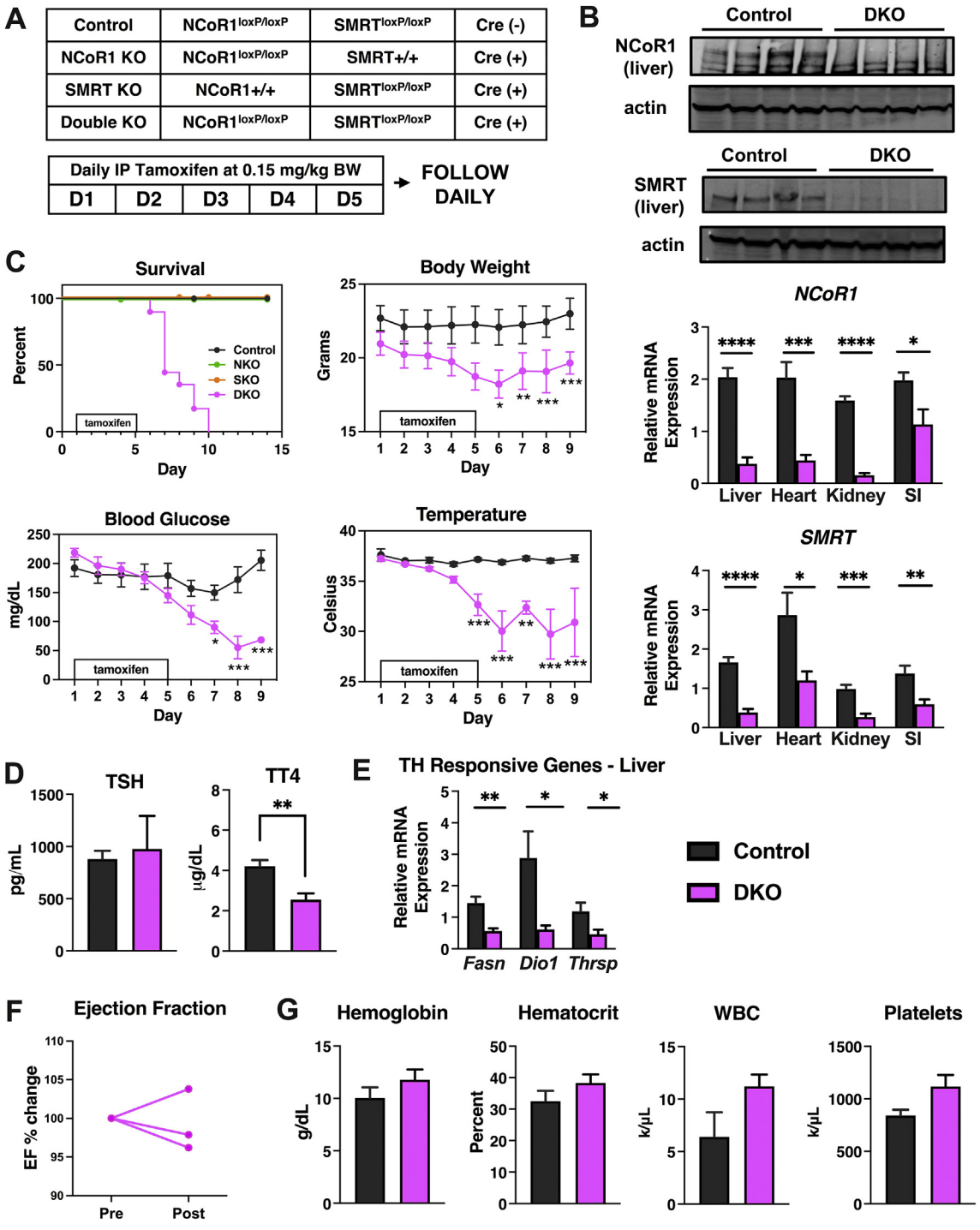

Figure 1: Postnatal deletion of NCOR1 and SMRT is lethal. (A) Shown are the genotypes that were studied (control (n = 15), NCOR1 and SMRT single KO (n = 5), NCOR1/SMRT DKO, (n = 6). Tamoxifen was administered for five days between weeks 8 and 9 in male mice. (B) Protein extracts from the liver of the indicated genotypes were probed with NCOR1 or SMRT antibodies. Beta-actin was used as a control. (top panels). qPCR of liver, heart, kidneys, and small intestine (SI) for NCOR1 and SMRT were performed (bottom panels, n = 7–8 per genotype). (C) Percentage of mice from indicated genotypes that survived for 15 days and body weight, blood glucose, and temperature of the control and DKO mice (n = 15 control, 6 DKO and 5 NCOR1 KO and 5 SMRT KO). (D) Thyroid-stimulating hormone (TSH) levels were measured by ELISA and total thyroxine (TT4) levels were measured by radioimmunoassay (n = 15 control, 6 DKO). (E) qPCR of thyroid hormone–responsive genes (n = 6 per genotype). (F) Ejection fraction was measured by echocardiography before tamoxifen (pre) and one day after tamoxifen administration was completed (post) and percent change was determined (n = 3). (G) Blood for hematologic cell counts was assessed (n = 4–5 per genotype). Data are shown as mean +/− SEM *P < 0.05, **P < 0.01, ***P < 0.001, ****P < 0.0001, post-hoc two-way ANOVA for survival analysis, otherwise unpaired student t-test.

NCOR1 using rabbit polyclonal anti-NCOR1 antibody (PHQQ; generated against a C-terminal NCoR peptide as previously described; diluted at 1:250), rabbit polyclonal anti-SMRTe (06—891; Millipore Sigma; diluted at 1:500), or rabbit polyclonal anti-HDAC3 (ab7030; abcam; diluted at 1:2000) overnight at 4 °C with mouse monoclonal anti-beta-actin antibody (MA191399; Fisher Scientific; diluted at 1:10,000) for NCOR1 and SMRT/NCOR2 control or mouse monoclonal anti-hsp90a/b antibody (sc-13119, Santa Cruz Biotechnology; 1:5,000). Goat anti-rabbit Alexa Fluor Plus 680 (A32734; Invitrogen) and goat anti-mouse Alexa Fluor Plus 488 (A32723; Invitrogen) were used as secondary antibodies and incubated at room temperature for 90 min. Images were captured on ChemiDoc Touch MP (Bio-rad).

2.8. Glucose tolerance tests and pyruvate tolerance tests

Mice were fasted for 8 h, and then, 1 mg/g body weight of glucose or pyruvate was dissolved in sterile sodium chloride. Fasting blood glucose was drawn just before glucose administration, either by oral gavage or intraperitoneal injection using a glucometer (OneTouch Ultra, Lifescan, Johnson & Johnson). Glucose levels were checked over 2 h. Pyruvate was administered through intraperitoneal injection.

2.9. Absorption tests

Mice were fasted for 4 h before the administration of 20 mL/kg body weight FITC-dextran and 200 mL of D-xylose using kits (4013 and 6601; Chondrex, Inc.). Blood was drawn at 1 h and 3 h after gavage.

2.10. Echocardiography studies

Echocardiography was performed on awake mice through pretamoxifen administration and one day after the completion of a five-day course of tamoxifen using a Vivid 7 ultrasound (GE Healthcare) equipped with a 14 MHZ i13L probe. Parasternal short-axis images were recorded using both M-mode and 2D-mode imaging at the level of papillary muscles. Images were analyzed offline using EchoPACS software (GE Healthcare). The average of at least three measurements was used for every data point from each mouse.

2.11. Metabolic phenotyping

Mice are individually housed within the Promethion High-Definition Multiplexed Respirometry System for Mice (Sable Systems International). Metabolic cages are located within an ambient temperature and light-controlled environmental enclosure, DB034-LT Laboratory Incubator (Darwin Chambers Company). Mice are exposed to a 12 h light/dark cycle and ambient temperature of 22 °C. They are housed on pine chip bedding without nestlets and provided ad libitum access to food and acidified water. Energy expenditure is assessed using indirect calorimetry and calculated using the Weir equation (3.941 kcal/L x VO2 + 1.106 kcal/L x VCO2 [20]. Respirometry values are determined every 5 min; the dwell time for each cage is 30 s, with 30-sec baseline cage sampling frequency that occurs every four cages. Rates of oxygen consumption and carbon dioxide production are acquired with a sampling frequency of 1 s. Respiratory exchange ratios (RER) are calculated as VCO2/VO2. Food and water intake along with body mass are assessed gravimetrically. Distance traveled (activity) is determined by XY position displacements that are represented by beam breaks (PedMeters and AllMeters). Body composition was analyzed by EchoMRI immediately after CO2 asphyxiation (EchoMRI™ Body Composition Analyzer).

2.12. Oxygen bomb calorimetry

All fecal pellets were collected from the bottom of metabolic cages, one mouse per cage, and total mass was recorded. Fecal pellets were dried at ~60 °C and total mass was recorded. Bomb calorimetry was performed in accordance with the manufacturer's directions. Three samples from each mouse were weighed and tested. Data were analyzed as previously described using an oxygen bomb calorimeter (Parr 6765 Combination Calorimeter, Parr Instrument Company) [21].

2.13. Histology and morphometric analysis

Paraffin-embedded sections were used for routine H and E staining. Small intestines were isolated and flushed with cold PBS. Villus height of jejunum was assessed using Image J Fiji.

2.14. Statistical analysis

Statistical analysis was performed using GraphPad Prism, version 7. All gene expression and hormonal analyses were performed on indicated group numbers in figure legends. The differences in mRNA expression, lipid levels, hormone levels, body composition were analyzed by Student's *t*-test. Bodyweight, blood glucose, body temperature, GTT, and PTT were analyzed by two-way ANOVA with repeated measures followed by Bonferroni test as *post-hoc* test. The log-rank test was used for survival analysis. Data are expressed as mean ± SEM and p values smaller than 0.05 were considered as statistically significant.

3. RESULTS

3.1. Postnatal global deletion of NCOR1 and SMRT is rapidly lethal

As discussed, embryonic deletion of NCOR1 or SMRT is lethal [12,13]. To study the effects of NCOR1 and SMRT KO in the adult mouse, we crossed $NCOR1^{loxP/+}$ mice or $SMRT^{loxP/+}$ mice with $NCOR1^{loxP/+}$ mice or $SMRT^{loxP/+}$ mice that expressed tamoxifen-inducible Cre (UBC-Cre-ERT2) [6,22,23]. This generated control mice ($NCOR1^{loxp/loxp}SMRT^{loxp/loxp}$), NCOR1 single KO, SMRT single KO, and NCOR1 and SMRT double KO (DKO) mice (Figure 1A). Beginning at age 8—9 weeks, adult male mice underwent intraperitoneal injection with 0.15 mg/kg body weight of tamoxifen for five days, which led to the deletion of NCOR1 and SMRT in the liver and other tissues (Figure 1B). Strikingly, a rapidly lethal phenotype developed in the DKO mice heralded by weight loss, hypothermia, and hypoglycemia was not observed in either the NCOR1 single KO, SMRT single KO, or control mice such that by day 10, all DKO mice had succumbed (Figure 1C). This was also observed in female mice who underwent the same protocol of tamoxifen injection at the same age as the male mice (Suppl. Figure 1). As NCOR1 and SMRT are key corepressors of the thyroid hormone receptor, and NCOR1 mediates sensitivity to TH, we next assessed thyroid function tests [6,8]. Thyroid-stimulating hormone (TSH) levels were unchanged between control and DKO mice, while total thyroxine levels (TT4) were significantly reduced (Figure 1D). This correlated with a reduction in the expression of thyroid hormone—responsive genes, *Fasn, Dio1,* and *Thrsp* in the livers of the DKO mice (Figure 1E). Importantly, this phenotype was not consistent with increased sensitivity to TH, which occurs in NCOR1 single KO mice, but instead was consistent with the euthyroid sick syndrome and the rapid induction of compensatory tissue hypothyroidism.

Because embryonic lethality from SMRT deletion is secondary to cardiac failure, we next assessed cardiac function in the DKO mice. As shown in Figure 1F, ejection fraction (EF) was monitored before tamoxifen administration and one day after tamoxifen treatment completion (equivalent to day 6 in Figure 1A). At this time point, the DKO mice were symptomatic, yet their EF's were preserved. Additionally, because embryonic deletion of NCOR1 leads to severe hematologic

abnormalities, we performed a complete blood count which showed no significant differences between hemoglobin levels, hematocrit, white blood cell count, and platelet count of DKO mice compared to controls (Figure 1G). Female mice also showed no change in EF or hemoglobin levels, though only a limited number were studied (Suppl. Figure 1).

3.2. Histone deacetylase 3 is stabilized by the corepressor complex and its knockout is not rapidly lethal

NCOR1 and SMRT function in part by recruiting histone deacetylase 3 (HDAC3) *in vivo*. However, the deacetylase-activating domains of NCOR1 and SMRT are conserved to interact with and activate HDAC3's deacetylase function and catalytic activity [16,24]. Additionally, NCOR1 and SMRT stabilize HDAC3 protein levels *in vitro* and *in vivo* [16,25]. Thus, we first examined HDAC3 protein and mRNA levels in DKO mice. As shown in Figure 2A, HDAC3 protein levels are reduced in the livers of DKO mice, but there is a compensatory increase in HDAC3 mRNA expression. To determine if the loss of HDAC3 was responsible for the phenotype of lethality in DKO mice, we generated postnatal HDAC3 KO mice alongside another cohort of DKO mice [24,26,27]. To perform this, we generated HDAC3$^{loxP/loxP}$ UBC Cre-ERT2 mice and treated them with tamoxifen for five days in tandem with NCOR1/SMRT DKO mice — with both groups having matched controls. After two weeks of

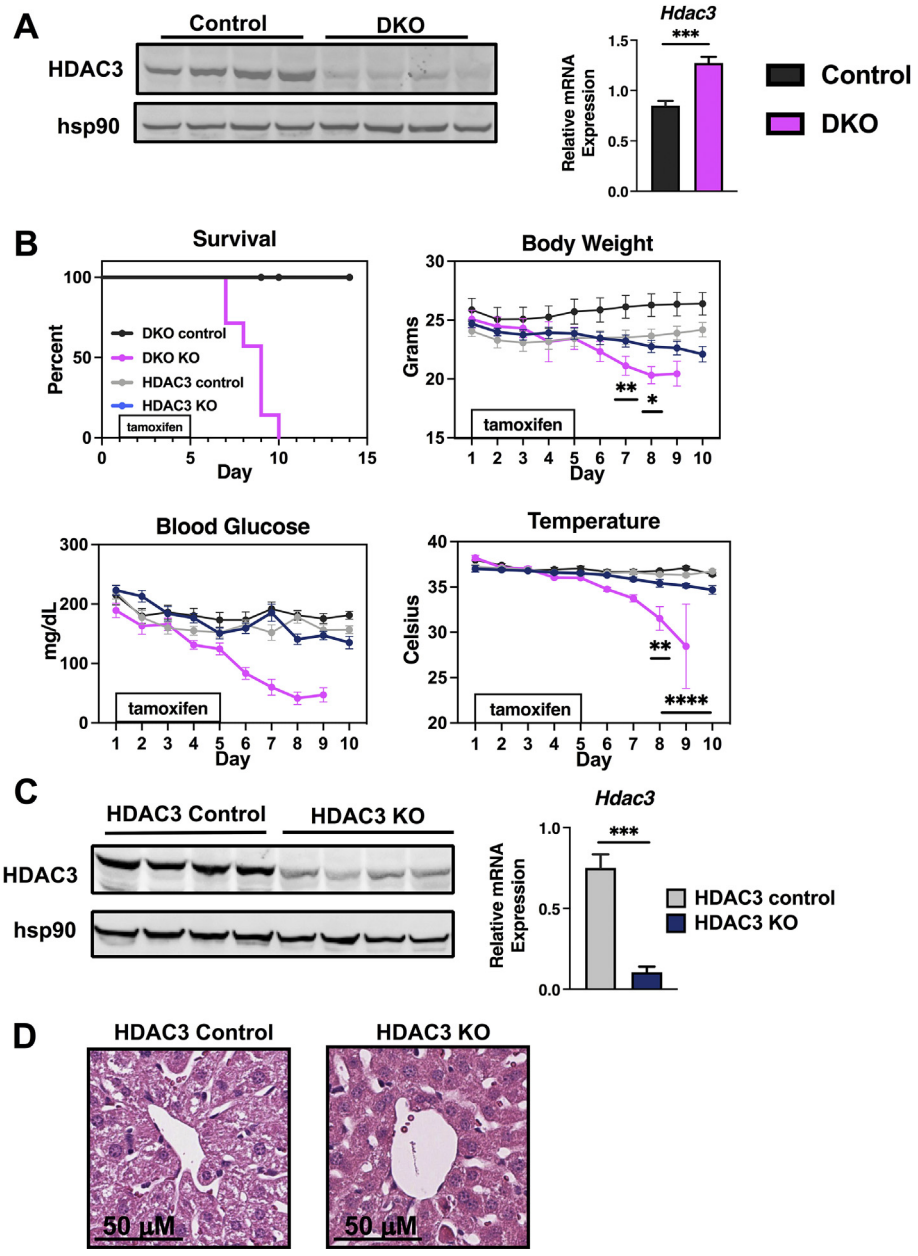

Figure 2: HDAC3 deletion postnatally does not lead to rapid lethality. (A) Protein extracts from the liver of the indicated genotypes were probed with an anti-HDAC3 antibody. Hsp90 was used as a control. Hdac3 liver mRNA levels were measured by qPCR (n = 8 per genotype). (B) Percentage of male mice from indicated genotypes surviving for 15 days and bodyweight, blood glucose, and temperature (n = 8–10 per genotype). (C) Protein extracts from the liver of the indicated genotypes were probed with an anti-HDAC3 antibody. Hsp90 was used as a control. (D) Liver tissue was fixed and hematoxylin and eosin staining was performed in the indicated genotype. Data are shown as mean +/− SEM, ***P < 0.001, post-hoc two-way ANOVA for survival analysis, otherwise unpaired student t-test.

daily monitoring, NCOR1/SMRT DKO mice all developed the same lethal phenotype of weight loss, hypoglycemia, and hypothermia within 10 days after tamoxifen injections start. While this phenotype was not observed in HDAC3 KO mice after 14 days and all were still alive, there was a trend toward weight loss, lower temperature, and lower blood glucose in HDAC3 KO mice; although this did not reach significance compared to their matched controls (Figure 2B). All HDAC3 KO mice had dramatically reduced HDAC3 protein and mRNA levels in the liver (Figure 2C). The histologic analysis did not reveal hepatosteatosis in the HDAC3 KO mice, which is known to be driven by the accumulation of triglycerides and is apparent in liver-specific HDAC3 KO mice (Figure 2D) [18].

3.3. NCOR1/SMRT DKO results in significant metabolic abnormalities

To further characterize the metabolic abnormalities observed in the NCOR1/SMRT DKO mice, we proceeded with metabolic phenotyping. A new cohort of male mice was given tamoxifen treatment as previously described. After the first injection of tamoxifen, mice were transferred to individual cages where they were acclimated for 48 h before data collection (Figure 3A). Surviving mice were sacrificed 48-h after the completion of tamoxifen treatment because of the rapid demise of the DKO mice, as previously noted. While total bodyweight was decreased by approximately 15% at this point, Echo-MRI showed that the reduction in total body mass was driven by a dramatic loss of fat mass in the DKO mice. Lean mass was significantly higher in the DKO mice compared to matched controls (Figure 3B). Food and water intake, adjusted for body weight, were significantly reduced in the DKO mice that began on day four of tamoxifen treatment (Figure 3C). Total energy expenditure was reduced from the start of day four of tamoxifen injections (Figure 3D), driven by a reduction during the dark cycle on day four, followed by a reduction in both light and dark cycles on days five and six (Suppl. Figure 2). The average respiratory exchange ratio was reduced in the DKO mice that began again on day four, driven by changes in oxygen consumption and carbon dioxide production in both light and dark cycles (Figure 3D and Suppl. Figure 2).

3.4. Glucose metabolism is altered in NCOR1/SMRT DKO mice

Glucose metabolism is significantly altered in the DKO mice as evidenced by the profound hypoglycemia that starts to develop early after tamoxifen administration. To evaluate the etiology further, DKO mice underwent oral glucose tolerance tests (OGTT), intraperitoneal glucose tolerance tests (IPGTT), and pyruvate tolerance tests (PTT). Given the rapid demise of the DKO mice and stress associated with fasting before these tests, we shortened the tamoxifen injection to four days, again beginning at age 8–9 weeks in male mice. Mice underwent 8 h of fasting before being subjected to an OGTT, IPGTT, or PTT on day five – one day after the completion of tamoxifen injection (Figure 4A). qPCR confirmed that four days of tamoxifen injection is sufficient to knockout NCOR1 and SMRT from the liver, which corresponds well to the protein levels of NCOR1 and SMRT (Suppl. Figure 3) and the actions of the Cre in other tissues (Figure 4B). DKO mice that underwent OGTT showed impairment in peak glucose levels attained at 15, 30, and 60 min after oral gavage of glucose. No difference was observed between groups at the start of 90 min or the end of the test at 120 min (Figure 4C). When the same protocol was followed on mice that underwent an IPGTT, no impairment was observed in peak glucose levels at 15 and 30 min post intraperitoneal injection. In the cohort undergoing IPGTT, DKO mice started at a significantly lower glucose level compared to control mice and DKO mice that underwent the OGTT (Figure 4D). DKO mice that underwent IPGTT had lower glucose levels compared to controls at 60, 90, and 120 min (Figure 4D). The area under the curve (AUC) calculations indicate a lower overall value in the DKO mice in both the OGTT and IPGTT (Figure 4C,D). We next evaluated gluconeogenesis using a pyruvate tolerance test (PTT). The same 4-day injection protocol preceded an 8-h fast and intraperitoneal injection of pyruvate one day after the completion of tamoxifen injections. Both control and DKO mice increased blood glucose by similar amounts. The reduced AUC in the DKO mice corresponds to their lower starting glucose levels (Figure 4E). Taken together, these data suggested that impairment could exist in nutrient absorption in male DKO mice that contributed to the observed hypoglycemia. However, no defect in the livers of DKO mice was observed in their ability to perform gluconeogenesis. Interestingly, when the same protocols were performed in female mice, no difference was observed between the OGTT and IPGTT, and the PTT was normal (Suppl. Figure 1).

To rule out detrimental regulatory hormone secretion, we examined fasting insulin levels and β-hydroxybutyrate levels, and no difference was observed either in control or DKO male mice (Figure 4F). A significant reduction in insulin levels in female DKO mice compared to control (Suppl. Figure 1D) indicate that in both male and female cohorts, hyperinsulinemia did not contribute to hypoglycemia. However, nonfasted Fgf21 mRNA expression levels were significantly increased in the livers of DKO mice, though only by 4-fold which is many-fold less than as observed in fully fasted mice—consistent with the fact that DKO mice still ate, though in decreased amounts, after the deletion of NCOR1 and SMRT (Figure 4G) [28]. A nonsignificant increase in Fgf21 mRNA levels was observed in the female cohorts (Suppl. Figure 1).

Finally, we examined gene expression in mice that had completed the full 5-day tamoxifen protocol (refer Figure 3A) to analyze key genes associated with glycolysis and gluconeogenesis. In the context of glycolysis, *Gck* was unchanged between groups, but both *Pfk* and *Pk* were significantly reduced in the DKO mice. However, no change was observed in total *Chrebp* expression or in the context of its alpha and beta isoforms (Figure 4H). Key enzymes in gluconeogenesis, including *G6pc, Fbp1,* and the transcription factor *Foxo1* were increased in DKO mice, while *Pdk1, Pck1,* and *Creb1* were unchanged (Figure 4I). Thus, the livers of DKO mice appeared to be compensating appropriately for the hypoglycemia observed, but not to a degree necessary to prevent the demise of DKO mice.

3.5. NCOR1/SMRT deletion leads to the rapid development of hepatosteatosis

Considering the profound hypoglycemia, we further examined the critical role of the liver in glucose metabolism and homeostasis, in addition to being a major target of thyroid hormone action. Hematoxylin and eosin staining showed the rapid development (within 10 days) of hepatosteatosis, both macrovesicular and microvesicular impact in the area surrounding the portal triad and central vein, respectively, in DKO mice (Figure 5A). This is definitively distinct from the lack of accumulation in HDAC3 KO mice. Lipid extraction from liver tissue of the mice showed that steatosis is driven primarily by an increase in hepatic triglyceride content of approximately 4-fold as there was no difference between cholesterol content (total and free) or phospholipids (Figure 5B). The increase in hepatic TG content was significantly higher than that observed in mice that have been fasted for 72 h [29]. Liver glycogen content in the DKO mice was significantly reduced, consistent with the observed hypoglycemia (Figure 5B). Gene expression analysis showed a mild increase in some markers of hepatic inflam-

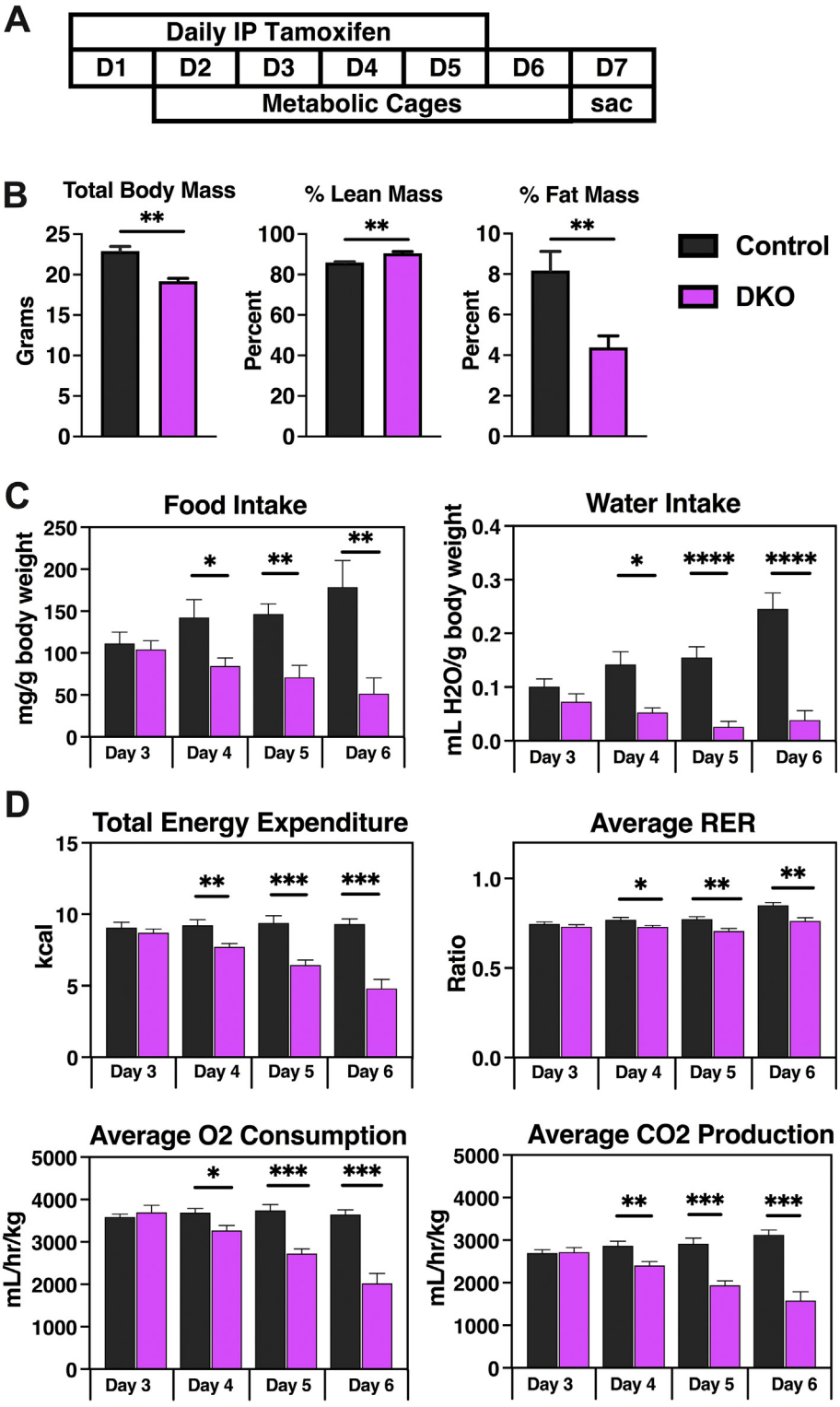

Figure 3: Metabolic phenotyping revealed significant changes in the DKO mice. (*A*) The metabolic phenotyping protocol is shown. (*B*) Total body mass, percent lean mass, and percent fat mass measured by echo-MRI. (*C*) Daily food intake and daily water intake, adjusted for body weight. (*D*) Daily total energy expenditure and average respiratory exchange ratio. (*E*) Total average oxygen consumption and carbon dioxide production adjusted for bodyweight. (n = 5 control, 8 DKO mice). Data are shown as mean +/− SEM *P < 0.05, **P < 0.01, ***P < 0.001, ****P < 0.0001, unpaired student t-test.

mation, including *CD14* and *Nqo1* in the DKO mice; but a reduction in *Lcn2* suggested that massive hepatic failure was not the cause of the demise of DKO mice and that steatosis did not lead to hepatic failure (Figure 5C). This was further supported by hepatic enzyme analysis where CK and AST were not different between control and DKO groups and ALT was only mildly increased in the DKO mice (Figure 5D). Key

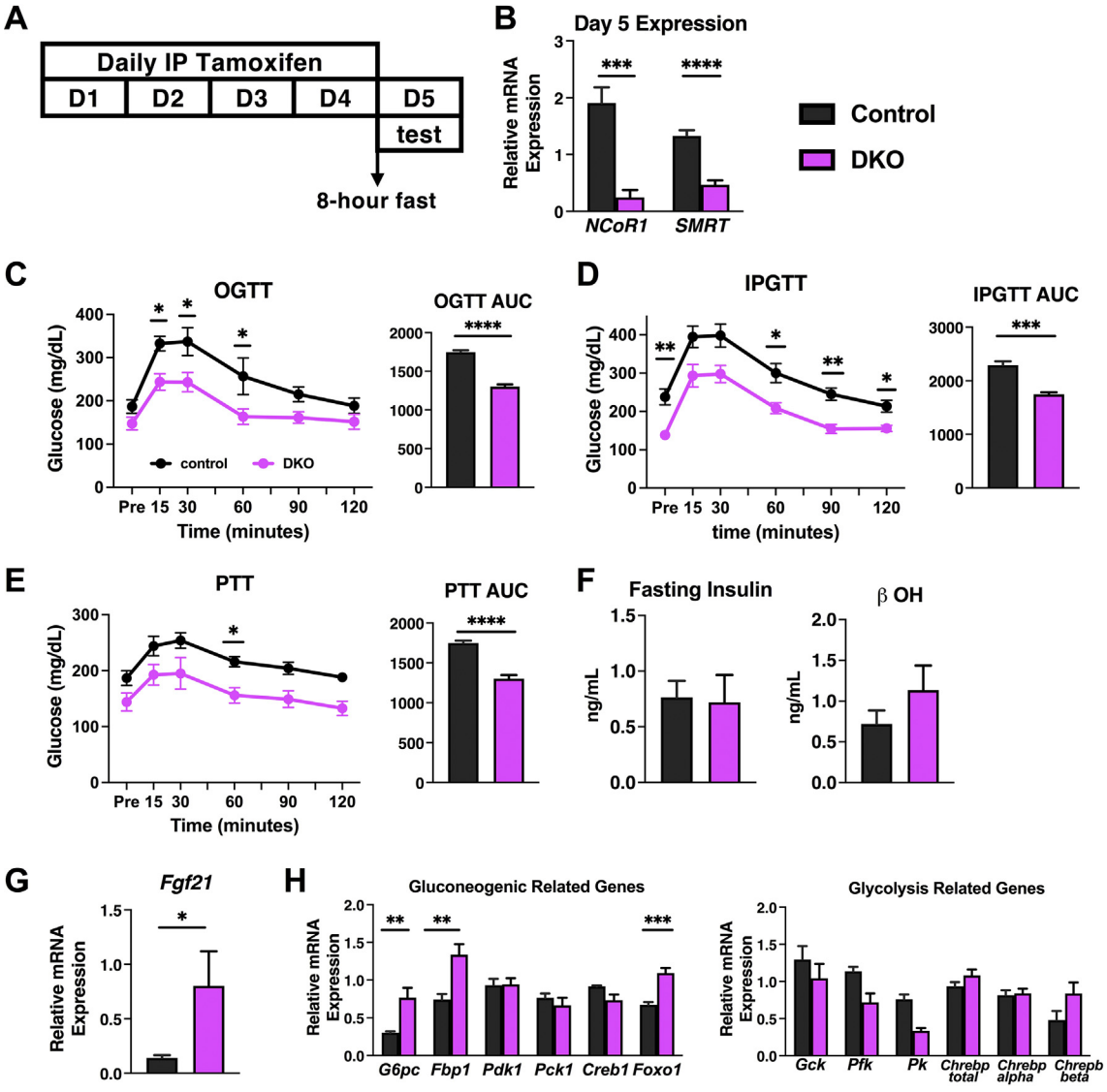

Figure 4: Glucose metabolism is altered in DKO mice. (*A*) Outline of glucose tolerance test and pyruvate tolerance test protocol. (*B*) mRNA was extracted from liver tissue and levels of NCOR1 and SMRT were measured by qPCR. (*C*) Oral glucose tolerance test (OGTT) was performed through oral gavage after an 8-h fast with corresponding AUC. (*D*) Intraperitoneal glucose tolerance test (IPGTT) was performed through intraperitoneal injection with corresponding AUC. (*E*) Pyruvate tolerance test (PTT) was performed by administering through intraperitoneal injection with corresponding AUC. (*F*) Fasting insulin and beta-hydroxybutyrate (b OH) levels were checked. (G) qPCR of Fgf21 was performed from hepatic mRNA. *(H)* mRNA was extracted from liver tissue from the groups that underwent metabolic phenotyping and genes related to glycolysis and gluconeogenesis were assessed. N = 7–8 mice per genotype for experiments B - G. N = 5 control, 8 DKO for H. Data are shown as mean +/− SEM *P < 0.05, **P < 0.01, ***P < 0.001, ****P < 0.0001, post-hoc two-way ANOVA and unpaired student t-test.

genes involved in both de novo lipogenesis and beta oxidation were also analyzed for their gene expression. *Srebp1c, Scd1,* and *Plin2*, were increased in DKO mice, but *Dgat1* and *Dgat2* were unchanged between the groups (Figure 5E). In terms of beta oxidation, *Cpt1α, Cpt1β, Cpt2,* and *Aox* were all significantly increased in DKO mice (Figure 5E). Levels of *Gpd1* were unchanged between control and DKO mice along with the levels of *Gys2* (Figure 5F). Serum levels of nonesterified fatty acids were similar between control and DKO mice, whereas serum triglyceride levels were significantly reduced in the DKO mice and no difference was observed between phospholipids and total or free cholesterol (Figure 5G). Thus, the hepatic steatosis present does not lead to significant liver dysfunction. The etiology is likely a combination of enhanced lipid synthesis and lipolysis because of the loss of fat mass. The increase in lipid synthesis could be responsible for increased glucose usage and contribute to hypoglycemia observed [30]. *Gpd1* couples carbohydrate and lipid metabolism and levels were not increased in DKO mice that suggest it is an alternate cause to hypoglycemia.

3.6. The intestine of DKO mice is structurally normal, but caloric absorption is impaired

As male DKO mice appeared to have a decreased ability to absorb glucose given orally, we next turned to the small intestine for analysis, considering its role in glucose transport and metabolism [31–33]. Histologic evaluation of the jejunum of the DKO mice that underwent metabolic phenotyping did not reveal any abnormalities (Figure 6A), and neither villi length in the jejunum nor total small intestine length was different between control and DKO mice

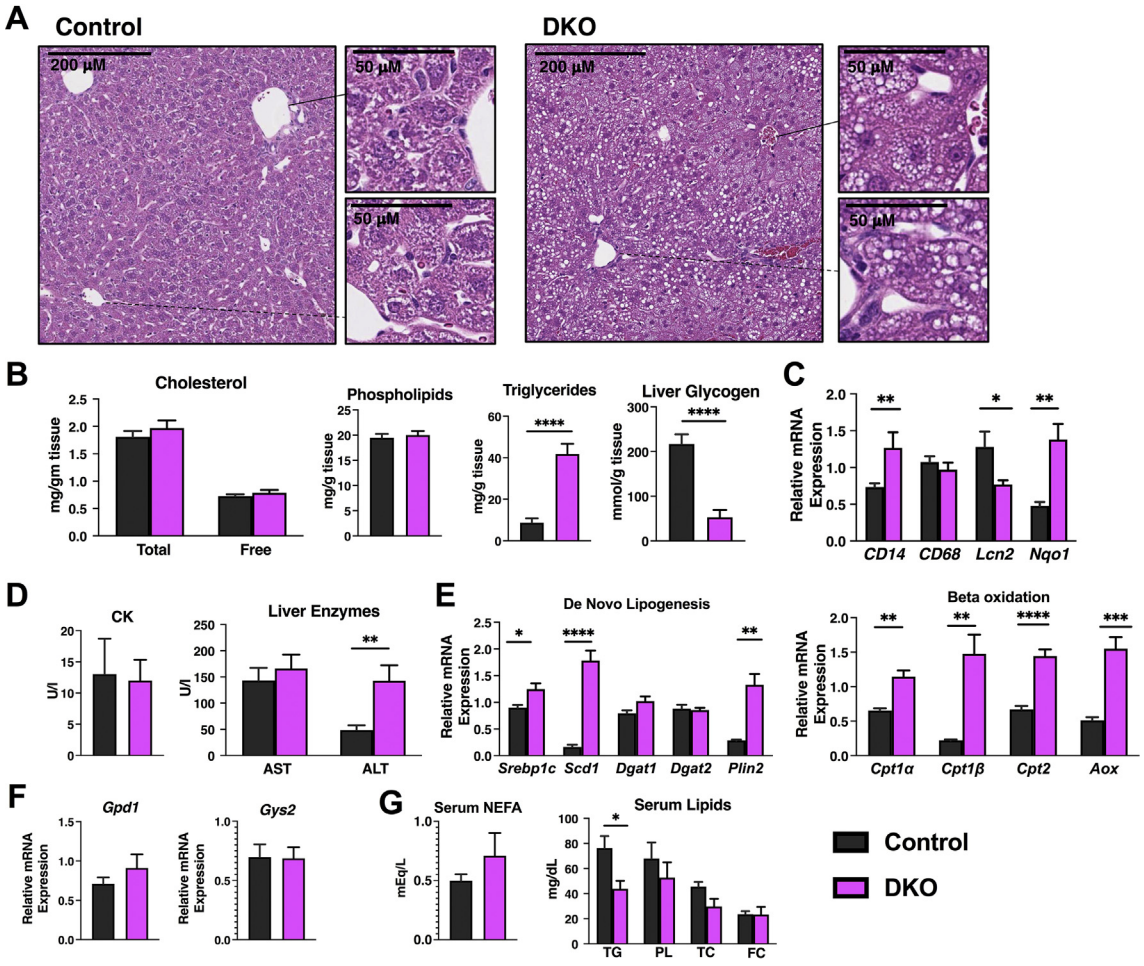

Figure 5: Hepatic function in DKO mice. (*A*) Liver tissue was fixed and hematoxylin and eosin staining was performed in the indicated genotypes. (*B*) Lipids and glycogen were extracted from liver tissue of the indicated genotypes. (*C*) Markers of liver inflammation were examined using qPCR. (*D*) Creatine kinase (CK), aspartate aminotransferase (AST), and alanine aminotransferase (ALT) were determined from serum from control and DKO mice. (*E*) Markers of de novo lipogenesis and beta-oxidation were determined by qPCR from the liver mRNA of control and DKO mice. *(F) Gpd1* and *Gys2 mRNA levels were determined by qPCR from* control and DKO mice. (*G*) Plasma nonesterified fatty acid (NEFA) levels and plasma lipids including triglyceride (TG), phospholipid (PL), total cholesterol (TC), and free cholesterol (FC) were determined. N = 5–8 mice per group. Data are shown as mean +/− SEM *P < 0.05, **P < 0.01, ***P < 0.001, ****P < 0.0001, unpaired student t-test.

(Figure 6B). Furthermore, visible food throughout the intestine was similar in both control and DKO mice on gross dissection. A 72-h caloric output, which was measured during metabolic phenotyping, was significantly lower in the DKO mice compared to controls (Figure6C). This was also true of fecal mass, but the average caloric density of the fecal matter was significantly increased in the DKO mice (Figure 6C). Thus, considering decreased food intake, it was evident that DKO mice were not as efficient in absorbing calories as the control animals. Indeed, the expression of glucose transporters was also significantly lower in the jejunum of DKO mice (Figure 6D).

To better assess intestinal transcellular and paracellular transport, control and DKO mice were subjected to the same tamoxifen injection protocol outlined in Figure 4A to perform D-xylose and FITC-Dextran absorption tests. The D-xylose absorption test, which measures transcellular intestinal uptake of sugars <342 Da, was not different between control and DKO mice as both absorbed similar amounts of D-xylose. FITC-Dextran absorption, which measures paracellular intestinal uptake of larger proteins >10,000 Da, was also not different between control and DKO mice (Figure 6E). Taken together, these results suggest that caloric loss in DKO fecal matter could accentuate the nutritional deprivation observed in these animals.

4. DISCUSSION

The knockout of both NCOR1 and SMRT, postnatally in mice is rapidly lethal, preceded by severe metabolic abnormalities. While both NCOR1 and SMRT are critical for normal embryonic development, the embryonic lethality associated with their deletion is distinctly different from the lethality observed with their postnatal combined deletion. The data presented suggest that NCOR1 and SMRT together overlap to control a program that regulates nutrient availability. Interestingly, when deleted individually, neither regulate nutrient availability nor SMRT deletion postnatally leads to profound obesity [11,34]. Thus, the NCOR1/SMRT pathway is likely to target a key set of pathways that control blood glucose levels that include targets in the liver and potentially the intestine. Whether central targets in the brain are also involved remains to be determined.

While embryonic and perinatal lethality are common in genetic ablation experiments, there are significantly fewer examples of postnatal

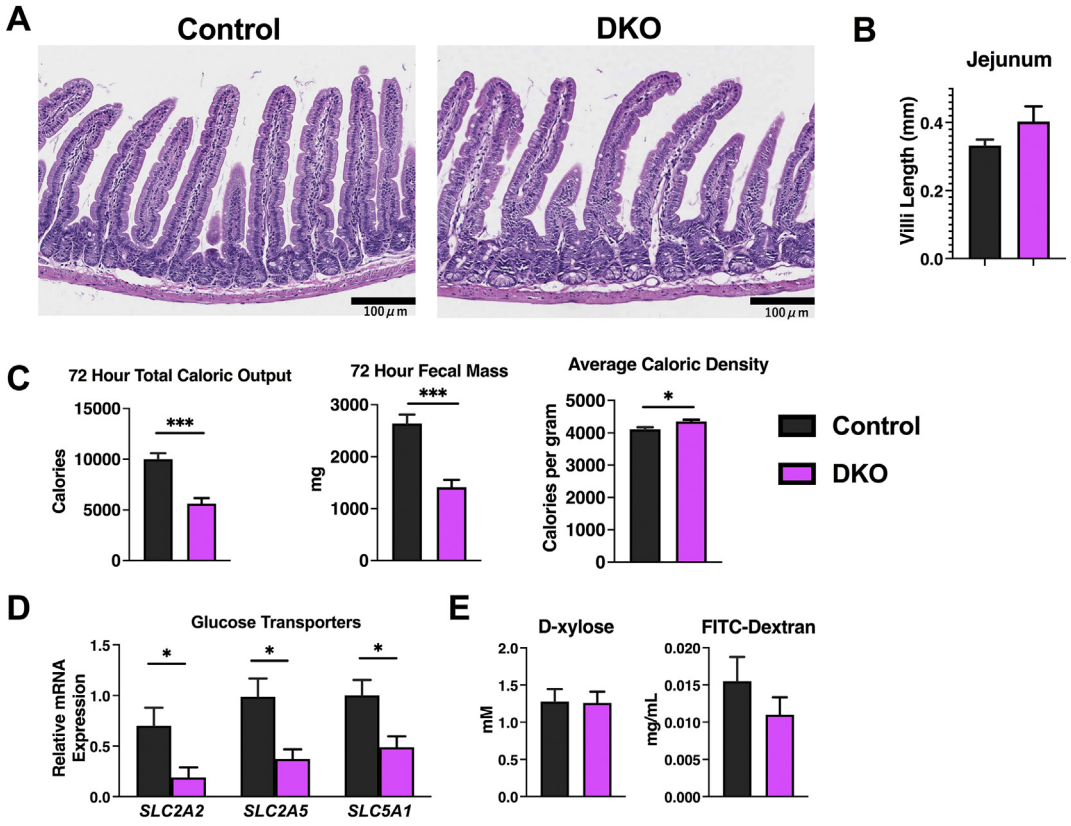

Figure 6: The jejunum of the small intestine is intact, but caloric absorption is impaired. (A) Hematoxylin and eosin staining of the jejunum from the indicated genotypes at the same level. (B) Villi length was measured within the jejunum using image J Fiji and displayed in mm. (C) A 72-h total caloric output, fecal mass, and average caloric density of the fecal mass was analyzed after bomb calorimetry. (D) mRNA was extracted from the small intestine at similar levels and glucose transporter levels were determined by qPCR. (E) The D-xylose and FITC-dextran absorption tests were performed on control and NCOR1/SMRT DKO mice. N = 5–8 mice per group. Data are shown as mean +/− SEM *P < 0.05, **P < 0.01, ***P < 0.001, ****P < 0.0001, unpaired student t-test.

deletion that causes lethality [35]. However, examples exist where the postnatal disruption of intestinal or hepatic function leads to a lethal phenotype. In the case of fat storage-inducing transmembrane protein 2 (FIT2/FIT2M) — a transmembrane endoplasmic reticulum protein that plays a role in lipid droplet formation — mice did not survive past two weeks of postnatal Cre-induction of FIT2/FIT2M deletion [36,37]. These mice developed a lethal malabsorptive enteropathy characterized by villus blunting, inhibition of intestinal stem cells, and crypt cell death [36]. While the FIT2/FIT2M KO mice have fasting hypoglycemia at day 10 and survive up to day 14 after the initiation of tamoxifen, NCOR1/SMRT DKO mice develop hypoglycemia earlier in the absence of fasting and they succumb earlier. Additionally, deletion of receptor-interacting protein kinase 1 (RIPK1) in the intestine of adult mice leads to death through intestinal cell destruction and presumably malabsorption [38,39]. However, we did not identify any histologic or malabsorptive abnormalities in the intestines of NCOR1/SMRT DKO mice, except for an increase in fecal caloric density noted on bomb calorimetry. In contrast to FIT2/FIT2M and NCOR1/SMRT DKO mice, postnatal deletion of liver kinase B1 (Lkb1), which mediates glucose and lipid metabolism, is lethal six weeks after Cre-induction [40,41]. Lkb1 KO mice started to lose weight two weeks after tamoxifen injection and had diminished quantities of brown and white adipose. However, they developed hyperglycemia and glucose intolerance [40]. All of these phenotypes share weight loss as a common feature, likely a unifying feature of a lethal phenotype.

A clear effector of NCOR1 and SMRT action is HDAC3. Deletion of HDAC3 postnatally from the heart leads to a severe phenotype and lethality only in the presence of a high-fat diet [25]. In the liver, deletion of HDAC3 causes significant hepatic steatosis [18]. When combined with hepatic-specific deletion of SREBP cleavage activating protein (SCAP), mice develop severe hypoglycemia, liver glycogen depletion, and high serum NEFA levels, and die within three weeks after their KO [42]. While the NCOR1/SMRT DKO mice do have liver glycogen depletion and hypoglycemia, β-hydroxybutyrate levels are unchanged from that of control mice and *fgf21* levels are only mildly increased—indicating mild fasting compared to HDAC3/SCAP KO mice [28]. Furthermore, unlike NCOR1/SMRT DKO mice, liver-specific HDAC3/SCAP KO mice also suffer from massive hepatic failure as evidenced by alanine transaminase levels >4000 mU/mL and significantly higher levels of inflammatory markers, including *Nqo1*, *Lcn2*, *Cd14*, and *Cd68,* compared NCOR1/SMRT DKO mice [42]. Finally, the postnatal deletion of HDAC3 globally does not lead to an acutely lethal phenotype as observed in the NCOR1/SMRT DKO mice, suggesting that NCOR1 and SMRT may regulate a pathway independent of HDAC3 that controls nutrient availability or usage. This is supported by the rapidity of hepatosteatosis development in NCOR1/SMRT DKO mice as compared to HDAC3 deleted mice. This would be in contrast to the epidermis where NCOR1 and SMRT control a similar pathway of differentiation to HDAC3 [16].

To further analyze the development of hypoglycemia in NCOR1/SMRT DKO mice, we observed several pathways in glucose metabolism. Not surprisingly, key hepatic enzymes of gluconeogenesis are increased as a result of compensation because of hypoglycemia. Additionally, the results of the pyruvate tolerance test point to gluconeogenic machinery being intact and functional in DKO mice. In contrast, gene expression of key enzymes and transcription factors that partake in glycolysis are downregulated, likely secondary to hepatic glycogen store depletion and a lack of substrate for participation in glycolysis. These results are consistent with relatively mild defects in liver function in DKO mice, despite the rapid development of hepatosteatosis in this model. Furthermore, glucose uptake from the small intestine appears to be impaired based on intraperitoneal and oral glucose tolerance tests in male mice as glucose absorption orally appears to be impaired 15 and 30 min after glucose administration. Also, bomb calorimetry data suggests that increased calories are being lost in the GI tract. Thus, while food intake is lower in DKO mice, it appears that an additional barrier is caloric absorption. In contrast to the glucose intolerance and insulin resistance observed in total body SMRT KO mice that develop obesity, DKO mice show no evidence of either of these [11]. Lastly, these mice do not appear to secrete excessive amounts of insulin that lead to hypoglycemia.

Finally, we looked at thyroid function in these mice considering the role of NCOR1 in mediating TH sensitivity mediation and the HPT axis control. However, mice that lack NCOR1 function because of an NCOR1 allele expression that cannot interact with the TR, have lower TH levels with a normal TSH; yet increased energy expenditure and enhanced TH-responsive gene expression [8]. These findings are consistent with enhanced sensitivity to thyroid hormone. Similarly, DKO mice also have a reduction in TH levels with a normal TSH. However, TH responsive gene expression is reduced in DKO mice. This pattern of thyroid function appears to be most consistent with nonthyroidal illness or the euthyroid sick syndrome, a condition observed in humans who are severely ill, consistent with the phenotype of the DKO mice [43]. Thus, an aberrantly activated thyroid axis does not appear to contribute to the weight loss or rapid demise of the DKO mice. Instead, the mice appropriately down-regulate TH levels in an attempt to lower metabolic demand.

In addition to the mechanisms explored, the global deletion of NCOR1 and SMRT impacts a variety of other signaling systems, given their ability to interact with a variety of nuclear receptors and other transcription factors in multiple tissues [2,44]. This includes, but is not limited to, hepatic estrogen receptor alpha that impacts metabolic pathways in the liver [45–47]. Future strategies to target nuclear receptors that interact with NCOR1 and SMRT would give further insight into selective pathway activation. This could be explored by studying the inactivation of individual nuclear receptors either genetically or through the use of antagonists — in addition to the deletion of NCOR1 and SMRT to identify pathways unique to the nuclear receptor. While other tissues may play a role in the rapid lethality of this model, our data taken together suggest that severe hypoglycemia led to death in these animals. We hypothesize that a combination of diminished food intake, coupled with poor absorption and a lack of available substrate led to the rapid lowering of blood glucose levels and consequent hypothermia. Further studies are required to focus on cell-specific replacement of corepressor function to determine the etiology of the novel pathways regulated.

AUTHOR CONTRIBUTIONS

Megan J. Ritter: Data curation, formal analysis, and writing - original draft and subsequent revisions.
Izuki Amano: Data curation, formal analysis, review and editing of the article.
Norihiro Imai: Data curation, formal analysis, review and editing of the article.
Lorraine de Oliveira: Data curation, formal analysis, and review of the article.
Kristen R. Vella: Reviewed and edited the article.
Anthony N. Hollenberg: Conceptualization, funding acquisition and resources, supervision of the project, data analysis and review, writing — original draft, review, and editing.

ACKNOWLEDGMENTS

This study was supported by NIDDK grant DK016523 (ANH) and the American Thyroid Association Thyroid Research Grant (MR). We thank Scott Hiebert for the HDAC3$^{loxP/loxP}$ mice, Ron Cohen for the SMRT$^{loxP/loxP}$ mice, Johan Auwerx for the NCOR1$^{loxp/loxp}$ mice, the Weill Cornell Medicine Metabolic Phenotyping Center, Dr. Munehiko Shibata for his assistance with echocardiograms, and Mr. Andrew Sangho Lee for his work on the western blots.

CONFLICT OF INTEREST

We declare that no competing interests exist.

APPENDIX ASUPPLEMENTARY DATA

Supplementary data to this article can be found online at https://doi.org/10.1016/j.molmet.2021.101315.

REFERENCES

[1] Astapova, I., 2016. Role of co-regulators in metabolic and transcriptional actions of thyroid hormone. Journal of Molecular Endocrinology 56(3):73–97.
[2] Mottis, A., Mouchiroud, L., Auwerx, J., 2013. Emerging roles of the co-repressors NCOR1 and SMRT in homeostasis. Genes & Development 27(8): 819–835.
[3] Costa-e-Sousa, R.H., Astapova, I., Ye, F., Wondisford, F.E., Hollenberg, A.N., 2012. The thyroid axis is regulated by NCOR1 via its actions in the pituitary. Endocrinology 153(10):5049–5057.
[4] Vella, K.R., Ramadoss, P., Costa, E.S.R.H., Astapova, I., Ye, F.D., Holtz, K.A., et al., 2014. Thyroid hormone signaling in vivo requires a balance between coactivators and corepressors. Molecular and Cellular Biology 34(9):1564–1575.
[5] Stanya, K.J., Kao, H.Y., 2009. New insights into the functions and regulation of the transcriptional corepressors SMRT and N-CoR. Cell Division 4:7.
[6] Shimizu, H., Astapova, I., Ye, F., Bilban, M., Cohen, R.N., Hollenberg, A.N., 2015. NCOR1 and SMRT play unique roles in thyroid hormone action in vivo. Molecular and Cellular Biology 35(3):555–565.
[7] Astapova, I., Lee, L.J., Morales, C., Tauber, S., Bilban, M., Hollenberg, A.N., 2008. The nuclear corepressor, NCoR, regulates thyroid hormone action in vivo. Proceedings of the National Academy of Sciences of the U S A 105(49): 19544–19549.
[8] Astapova, I., Vella, K.R., Ramadoss, P., Holtz, K.A., Rodwin, B.A., Liao, X.H., et al., 2011. The nuclear receptor corepressor (NCoR) controls thyroid hormone sensitivity and the set point of the hypothalamic-pituitary-thyroid axis. Molecular Endocrinology 25(2):212–224.
[9] Mendoza, A., Astapova, I., Shimizu, H., Gallop, M.R., Al-Sowaimel, L., MacGowan, S.M.D., et al., 2017. NCoR1-independent mechanism plays a role in the action of the unliganded thyroid hormone receptor. Proceedings of the National Academy of Sciences of the U S A 114(40):E8458–E8467.

[10] Fozzatti, L., Lu, C., Kim, D.W., Park, J.W., Astapova, I., Gavrilova, O., et al., 2011. Resistance to thyroid hormone is modulated in vivo by the nuclear receptor corepressor (NCOR1). Proceedings of the National Academy of Sciences of the U S A 108(42):17462–17467.
[11] Shimizu, H., Lu, Y., Vella, K.R., Damilano, F., Astapova, I., Amano, I., et al., 2019. Nuclear corepressor SMRT is a strong regulator of body weight independently of its ability to regulate thyroid hormone action. PloS One 14(8): e0220717.
[12] Jepsen, K., Hermanson, O., Onami, T.M., Gleiberman, A.S., Lunyak, V., McEvilly, R.J., et al., 2000. Combinatorial roles of the nuclear receptor corepressor in transcription and development. Cell 102(6):753–763.
[13] Jepsen, K., Gleiberman, A.S., Shi, C., Simon, D.I., Rosenfeld, M.G., 2008. Cooperative regulation in development by SMRT and FOXP1. Genes & Development 22(6):740–745.
[14] Bhaskara, S., Chyla, B.J., Amann, J.M., Knutson, S.K., Cortez, D., Sun, Z.W., et al., 2008. Deletion of histone deacetylase 3 reveals critical roles in S phase progression and DNA damage control. Molecular Cell 30(1):61–72.
[15] Montgomery, R.L., Potthoff, M.J., Haberland, M., Qi, X., Matsuzaki, S., Humphries, K.M., et al., 2008. Maintenance of cardiac energy metabolism by histone deacetylase 3 in mice. Journal of Clinical Investigation 118(11):3588–3597.
[16] Szigety, K.M., Liu, F., Yuan, C.Y., Moran, D.J., Horrell, J., Gochnauer, H.R., et al., 2020. HDAC3 ensures stepwise epidermal stratification via NCoR/SMRT-reliant mechanisms independent of its histone deacetylase activity. Genes & Development 34(13–14):973–988.
[17] Feng, D., Liu, T., Sun, Z., Bugge, A., Mullican, S.E., Alenghat, T., et al., 2011. A circadian rhythm orchestrated by histone deacetylase 3 controls hepatic lipid metabolism. Science 331(6022):1315–1319.
[18] Sun, Z., Miller, R.A., Patel, R.T., Chen, J., Dhir, R., Wang, H., et al., 2012. Hepatic Hdac3 promotes gluconeogenesis by repressing lipid synthesis and sequestration. Nature Medicine 18(6):934–942.
[19] Alves-Bezerra, M., Li, Y., Acuna, M., Ivanova, A.A., Corey, K.E., Ortlund, E.A., et al., 2019. Thioesterase superfamily member 2 promotes hepatic VLDL secretion by channeling fatty acids into triglyceride biosynthesis. Hepatology 70(2):496–510.
[20] Weir, J.B., 1949. New methods for calculating metabolic rate with special reference to protein metabolism. J Physiol 109(1–2):1–9.
[21] Grobe, J.L., 2017. Comprehensive assessments of energy balance in mice. Methods in Molecular Biology 1614:123–146.
[22] Yamamoto, H., Williams, E.G., Mouchiroud, L., Canto, C., Fan, W., Downes, M., et al., 2011. NCOR1 is a conserved physiological modulator of muscle mass and oxidative function. Cell 147(4):827–839.
[23] Feil, R., Wagner, J., Metzger, D., Chambon, P., 1997. Regulation of Cre recombinase activity by mutated estrogen receptor ligand-binding domains. Biochemical and Biophysical Research Communications 237(3):752–757.
[24] Sun, Z., Feng, D., Fang, B., Mullican, S.E., You, S.H., Lim, H.W., et al., 2013. Deacetylase-independent function of HDAC3 in transcription and metabolism requires nuclear receptor corepressor. Mol Cell 52(6):769–782.
[25] Sun, Z., Singh, N., Mullican, S.E., Everett, L.J., Li, L., Yuan, L., et al., 2011. Diet-induced lethality due to deletion of the Hdac3 gene in heart and skeletal muscle. Journal of Biological Chemistry 286(38):33301–33309.
[26] You, S.H., Lim, H.W., Sun, Z., Broache, M., Won, K.J., Lazar, M.A., 2013. Nuclear receptor co-repressors are required for the histone-deacetylase activity of HDAC3 in vivo. Nature Structural & Molecular Biology 20(2): 182–187.
[27] Wen, Y.D., Perissi, V., Staszewski, L.M., Yang, W.M., Krones, A., Glass, C.K., et al., 2000. The histone deacetylase-3 complex contains nuclear receptor corepressors. Proceedings of the National Academy of Sciences of the U S A 97(13):7202–7207.
[28] Badman, M.K., Pissios, P., Kennedy, A.R., Koukos, G., Flier, J.S., Maratos-Flier, E., 2007. Hepatic fibroblast growth factor 21 is regulated by PPARalpha and is a key mediator of hepatic lipid metabolism in ketotic states. Cell Metabolism 5(6):426–437.
[29] Hashimoto, T., Cook, W.S., Qi, C., Yeldandi, A.V., Reddy, J.K., Rao, M.S., 2000. Defect in peroxisome proliferator-activated receptor alpha-inducible fatty acid oxidation determines the severity of hepatic steatosis in response to fasting. Journal of Biological Chemistry 275(37):28918–28928.
[30] Uyeda, K., Repa, J.J., 2006. Carbohydrate response element binding protein, ChREBP, a transcription factor coupling hepatic glucose utilization and lipid synthesis. Cell Metabolism 4(2):107–110.
[31] Gorboulev, V., Schurmann, A., Vallon, V., Kipp, H., Jaschke, A., Klessen, D., et al., 2012. Na(+)-D-glucose cotransporter SGLT1 is pivotal for intestinal glucose absorption and glucose-dependent incretin secretion. Diabetes 61(1): 187–196.
[32] Zhang, F., Wan, H., Chu, F., Lu, C., Chen, J., Dong, H., 2021. Small intestinal glucose and sodium absorption through calcium-induced calcium release and store-operated Ca(2+) entry mechanisms. British Journal of Pharmacology 178:346–362.
[33] Penhoat, A., Fayard, L., Stefanutti, A., Mithieux, G., Rajas, F., 2014. Intestinal gluconeogenesis is crucial to maintain a physiological fasting glycemia in the absence of hepatic glucose production in mice. Metabolism 63(1):104–111.
[34] Nofsinger, R.R., Li, P., Hong, S.H., Jonker, J.W., Barish, G.D., Ying, H., et al., 2008. SMRT repression of nuclear receptors controls the adipogenic set point and metabolic homeostasis. Proceedings of the National Academy of Sciences of the U S A 105(50):20021–20026.
[35] Brown, S.D., Moore, M.W., 2012. The International Mouse Phenotyping Consortium: past and future perspectives on mouse phenotyping. Mammalian Genome 23(9–10):632–640.
[36] Goh, V.J., Tan, J.S., Tan, B.C., Seow, C., Ong, W.Y., Lim, Y.C., et al., 2015. Postnatal deletion of fat storage-inducing transmembrane protein 2 (FIT2/FITM2) causes lethal enteropathy. Journal of Biological Chemistry 290(42): 25686–25699.
[37] Kadereit, B., Kumar, P., Wang, W.J., Miranda, D., Snapp, E.L., Severina, N., et al., 2008. Evolutionarily conserved gene family important for fat storage. Proceedings of the National Academy of Sciences of the U S A 105(1):94–99.
[38] Takahashi, N., Vereecke, L., Bertrand, M.J., Duprez, L., Berger, S.B., Divert, T., et al., 2014. RIPK1 ensures intestinal homeostasis by protecting the epithelium against apoptosis. Nature 513(7516):95–99.
[39] Dillon, C.P., Weinlich, R., Rodriguez, D.A., Cripps, J.G., Quarato, G., Gurung, P., et al., 2014. RIPK1 blocks early postnatal lethality mediated by caspase-8 and RIPK3. Cell 157(5):1189–1202.
[40] Shan, T., Xiong, Y., Kuang, S., 2016. Deletion of Lkb1 in adult mice results in body weight reduction and lethality. Scientific Reports 6:36561.
[41] Khayati, K., Bhatt, V., Hu, Z.S., Fahumy, S., Luo, X., Guo, J.Y., 2020. Autophagy compensates for Lkb1 loss to maintain adult mice homeostasis and survival. Elife 9.
[42] Papazyan, R., Sun, Z., Kim, Y.H., Titchenell, P.M., Hill, D.A., Lu, W., et al., 2016. Physiological suppression of lipotoxic liver damage by complementary actions of HDAC3 and SCAP/SREBP. Cell Metabolism 24(6):863–874.
[43] Fliers, E., Boelen, A., 2021. An update on non-thyroidal illness syndrome. Journal of Endocrinological Investigation 44:1597–1607.
[44] Kang, Z., Fan, R., 2020. PPARalpha and NCOR/SMRT corepressor network in liver metabolic regulation. The FASEB Journal 34(7):8796–8809.
[45] Qiu, S., Vazquez, J.T., Boulger, E., Liu, H., Xue, P., Hussain, M.A., et al., 2017. Hepatic estrogen receptor alpha is critical for regulation of gluconeogenesis and lipid metabolism in males. Scientific Reports 7(1):1661.
[46] Della Torre, S., Mitro, N., Meda, C., Lolli, F., Pedretti, S., Barcella, M., et al., 2018. Short-term fasting reveals amino acid metabolism as a major sex-discriminating factor in the liver. Cell Metabolism 28(2):256–267 e255.
[47] Meda, C., Barone, M., Mitro, N., Lolli, F., Pedretti, S., Caruso, D., et al., 2020. Hepatic ERalpha accounts for sex differences in the ability to cope with an excess of dietary lipids. Molecular Metabolism 32:97–108.

